Theoretical formalism and experimental verification of line shapes of NMR intermolecular multiple-quantum coherence spectra

Bingwen Zheng, Zhong Chen, Shuhui Cai, Jianhui Zhong, and Chaohui Ye

Citation: J. Chem. Phys. **123**, 074317 (2005); doi: 10.1063/1.2001652

View online: http://dx.doi.org/10.1063/1.2001652

View Table of Contents: http://jcp.aip.org/resource/1/JCPSA6/v123/i7

Published by the American Institute of Physics.

Theoretical formalism and experimental verification of line shapes of NMR intermolecular multiple-quantum coherence spectra

Bingwen Zheng, Zhong Chen,[a),b)] and Shuhui Cai
Department of Physics and State Key Laboratory of Physical Chemistry of Solid Surface, Xiamen University, Xiamen 361005, People's Republic of China and Department of Radiology, University of Rochester, Rochester, New York 14642

Jianhui Zhong
Departments of Radiology and Physics and Astronomy, University of Rochester, Rochester, New York 14642

Chaohui Ye[a),c)]
State Key Laboratory of Magnetic Resonance and Atomic and Molecular Physics, Wuhan Institute of Physics and Mathematics, The Chinese Academy of Science, Wuhan 430071, People's Republic of China

(Received 24 January 2005; accepted 27 June 2005; published online 24 August 2005)

Although the theories and potential applications of intermolecular multiple-quantum coherences (iMQCs) have been under active investigations for over a decade, discussion of iMQC NMR signal formation was mainly confined in the time domain. In this paper, a full line-shape theory was developed to describe iMQC signals in the frequency domain. Relevant features of the line shape, such as peak height, linewidth, and phase, were investigated in detail. Predictions based on the theory agree well with experimental and simulated results. Since radiation-damping effects always couple with iMQCs in highly polarized liquid-state NMR systems, and strongly radiation-damped signals have many spectral characteristics similar to those of iMQCs, a detailed comparison was also made between them from different spectral aspects. With detailed comparison of peak height, linewidth, and phase, this work demonstrates that the iMQC and radiation-damping phenomena result from two completely different physical mechanisms despite that both present similar signal features and coexist in highly polarized liquid-state NMR systems. © *2005 American Institute of Physics*. [DOI: 10.1063/1.2001652]

I. INTRODUCTION

Since the correlation spectroscopy (COSY) revamped by asymmetric z-gradients echo detection (CRAZED) sequence was proposed, theories and applications of intermolecular multiple-quantum coherences (iMQCs) have attracted a great interest in the past decade.[1–4] Similarly, multiple spin echoes (MSEs) can be observed in highly polarized systems, e.g., solid He,[5] liquid He,[6] and water.[7] Although iMQCs and MSEs differ significantly in their forms, it has been shown that both effects result from residual long-range intermolecular dipolar interactions. Either the quantum-mechanical density matrix[8–11] or classic dipolar field treatments[12,13] can interpret the physical characteristics of iMQC and MSE effects. A series of applications have been tested in magnetic resonance imaging (MRI),[3,14–17] structural measurements,[18,19] and high-resolution spectra in inhomogeneous fields.[2,20–22]

Both iMQCs and radiation damping cause previously unexpected effects in spin echo and generate harmonic peaks in two-dimensional NMR experiments.[1,23,24] Radiation-damping effects always couple with iMQCs in highly polarized liquid-state NMR systems,[25,26] and the envelopes of iMQC time-domain signals are quite similar to those of the radiation-damped ones.[8,27,28] Despite the fact that iMQC and radiation-damping effects result in similar signal characteristics and they coexist in samples with large magnetizations (such as proteins in water or even pure water) at high magnetic fields, their physical mechanisms are totally different.

To the best of our knowledge, most iMQC studies are confined to the time domain and the iMQC line shape in the frequency domain has not been investigated yet. Therefore, a mathematical derivation of iMQC line-shape functions was performed in this paper. Explicit expressions of iMQC line shape were developed in Sec. II. The results show that the iMQC signals in the frequency domain no longer yield pure Lorentzian or Gaussian line shape, but a line shape consisting of several basic functions, modulated by an oscillating cosine function. In spite of the similar spectral characteristics for iMQCs and radiation damping, our results indicate that their line-shape expressions in the frequency domain and the corresponding cosine functions which lead to line-shape distortion are grossly different. The relevant features of the spectral line shape were investigated in detail under the approximation of weak dipolar field effects. The peak height of nth coherence order is found to be dependent on the flip angle of the second radio-frequency (rf) pulse β in the CRAZED sequence and M_0 to the power n. The linewidths of iMQC spectra of different coherence orders are found to be independent of the flip angle β, completely different from that of the radiation-damping effect. The phase distortions of

[a)]Authors to whom correspondence should be addressed.
[b)]Electronic mail: chenz@jingxian.xmu.edu.cn
[c)]Electronic mail: ye@wipm.ac.cn

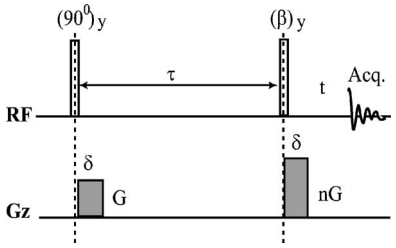

FIG. 1. The basic CRAZED pulse sequence for detecting iMQC signals in solution. The first gradient was applied immediately after the first rf pulse to reduce the radiation damping in the evolution period τ.

iMQC signals were explored mathematically and the derived line-shape expressions were verified by the comparison between the theoretical predictions, numerical simulations, and experimental observations in Sec. III. In Sec. IV, by tuning the probe to different extent, we introduced the radiation-damping effect of different strength and investigated how it influences the iMQC spectra. In experiments related to iMQCs, one can judge whether radiation damping is also active in an iMQC measurement by observing the negative-amplitude regions of the experimental spectra.

II. THEORETICAL FORMALISM

A. Time-domain signal

The original CRAZED sequence[4] shown in Fig. 1 is employed to excite the iMQC signals. Two field gradients with relative area of $1:n$ are used to select the n-quantum coherence signals; G and δ are the magnitude and duration of the gradients, respectively; γ is the gyromagnetic ratio; and τ and t are the time intervals of the evolution and detection periods, respectively. The dipolar field B_d makes the Bloch-Torrey equations nonlinear.[12,13] However, when a strong linear field gradient is applied only along a single direction z and the magnetization is spatially modulated on a length scale small compared to the structural sizes of the sample, the dipolar field at each point becomes a local function of the magnetization at the same point and thus simplify the spin dynamics.[7,29,30] Our discussions presented herein is confined to the approximation of weak dipolar field effects, as defined by $\gamma\mu_0 M_0 t \ll 1$,[7,29] to which most CRAZED experiments performed to date satisfy (in the above μ_0 is the magnetic permeability constant, and M_0 is the equilibrium magnetization per unit volume of the sample). When the transverse relaxation in the detection period is taken into account, the signals in the laboratory frame by solving the modified Bloch-Torrey equations including the dipolar field are given by

$$s(t) = i^{-n-1} M_0 \{ n J_n(\xi)/\xi - 0.5[J_{n-1}(\xi) - J_{n+1}(\xi)]\cos\beta \} e^{i\omega_0 t} e^{-t/T_2} \quad (n > 0), \tag{1}$$

$$s(t) = -iM_0 J_1(-\xi)\cos\beta e^{i\omega_0 t} e^{-t/T_2} \quad (n = 0), \tag{2}$$

where $\xi = te^{-\pi/T_2} e^{-(k^2 D + 1/T_1)t} \sin\beta/\tau_d$, in which the wave number is $k = \gamma G \delta$ and the demagnetization field time is $\tau_d = (\gamma\mu_0 M_0)^{-1}$,[8,9] and T_1, T_2, and D are the conventional longitudinal relaxation time, transverse relaxation time, and molecular diffusion coefficient, respectively. Equations (1) and (2) show that the signal is proportional to a nth-order Bessel function $J_n(\xi)$.[9] Unlike the envelopes of conventional free induction decays (FIDs) which satisfy a single-exponent decay, the envelopes of iMQC FIDs grow up from zero at $t=0$ before reaching their maximum amplitudes and then slowly decay to zero, as shown in Figs. 2(a)–2(d). Moreover, no matter how large the flip angle β of the second rf pulse is, the amplitude of FIDs at $t=0$ is always equal to zero. This characteristic is grossly different from that of radiation-damped FIDs.[27,28] When radiation damping becomes the dominant mechanism for the magnetization to return to the equilibrium state, the envelope of the radiation-damped FID is a truncated hyperbolical secant function [see Figs. 2(e)–2(h)].[27]

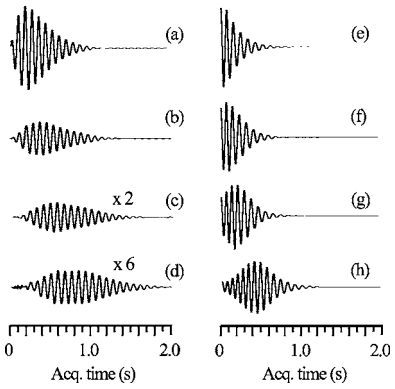

FIG. 2. FIDs of a sample with 50% H_2O and 50% D_2O. (a)–(d) iMQC FIDs from different coherence order: (a) $n=2$, (b) $n=3$, (c) $n=4$, and (d) $n=5$; (e)–(f) FIDs under strong radiation-damping conditions with different rf flip angle: (e) $\pi/2$, (f) $2\pi/3$, (g) $5\pi/6$, and (h) $35\pi/36$. Note that the behavior of iMQC FIDs is different from those of radiation-damped signals. Noticeably all iMQC FIDs start with zero amplitude.

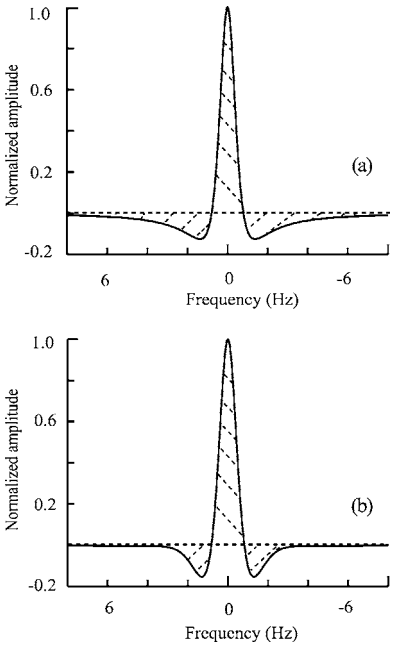

FIG. 3. Comparison of the theoretical spectra of (a) iMQC signal and (b) strong radiation-damped signal. A linewidth of 1.59 Hz is assumed for both spectra.

B. Fourier transformations of time-domain signal

As a special function in mathematics, the Bessel function $J_n(\xi)$ of integer order n has the following properties:[31]

$$J_{n-1}(\xi) - J_{n+1}(\xi) = 2\frac{d}{d\xi}[J_n(\xi)], \tag{3}$$

$$J_n(\xi) = \sum_{j=0}^{\infty} \frac{(-1)^j}{\Gamma(j+1)\Gamma(n+j+1)2^{2j+n}} \xi^{2j+n}, \tag{4}$$

where $\Gamma(j)$ is the gamma function defined by $\Gamma(j)=(j-1)!$ for integer j.[31] With the simplified processes using the expansion treatment of the Bessel function, the complex Fourier transform (FT) on FIDs can be obtained (see Appendix 1 in the supplementary material for details[32]),

$$S(\omega)|_{n>0} = i^{-n-1} M_0 \sum_{j=0}^{\infty} \frac{(-1)^{j+n}(e^{-\pi/T_2}\sin\beta/\tau_d)^{2j+n-1}}{\Gamma(j+1)\Gamma(n+j+1)2^{2j+n}} \times \frac{\Gamma(2j+n)[n-(2j+n)\cos\beta]}{\left\{\frac{1}{T_2} + (2j+n-1)[k^2D + 1/T_1] - i(\omega_0-\omega)\right\}^{2j+n}}, \tag{5}$$

$$S(\omega)|_{n=0} = iM_0 \sum_{j=0}^{\infty} \frac{(-1)^{j}(e^{-\pi/T_2}\sin\beta/\tau_d)^{2j+1}}{\Gamma(j+1)\Gamma(j+2)2^{2j+1}} \times \frac{\Gamma(2j+2)\cos\beta}{\left\{\frac{1}{T_2} + (2j+1)[k^2D + 1/T_1] - i(\omega_0-\omega)\right\}^{2j+2}}. \tag{6}$$

In practice, one is interested in an absorption mode spectrum that may be obtained by taking the real or the imaginary part of the complex spectrum in Eqs. (5) and (6), depending upon the value of n.[32] Our results show that an iMQC spectrum is a superposition of a series of lines which are non-Lorentzian or Gaussian [see Eqs. (a11)–(a14) in the supplementary material for details[32]]. Clearly, the line shapes are distorted by a cosine term as shown in Fig. 3(a) [the corresponding cosine terms can be found in Eqs. (a11) and (a12) of the supplementary material[32]]. The iMQC spectra are very similar to the radiation-damped ones, which are twisted by cosine functions [Fig. 3(b)].[27,28]

To further verify the inerrancy of Fourier transform, the integral of its Fourier transform was performed (see Appendix 2 in the supplementary material for details[32]) and was found to be equal to the first point ($t=0$) of iMQC FIDs, which is always zero. Therefore, the results manifest that the area of the positive-amplitude region in an iMQC peak [right-twilled region in Fig. 3(a)] must be equal to the area of the negative-amplitude region [left-twilled region in Fig. 3(a)] since the full integral of an iMQC peak is zero. However, for a radiation-damped peak, the area of the positive-amplitude region [right-twilled region in Fig. 3(b)] is always greater than the area of the negative-amplitude region [left-twilled region in Fig. 3(b)] unless the flip angle is π. When the flip angle is close to π, the first point of a radiation-damped FID is furthest away from the maximum amplitude of the FID envelope and the spectrum continuously oscillates.

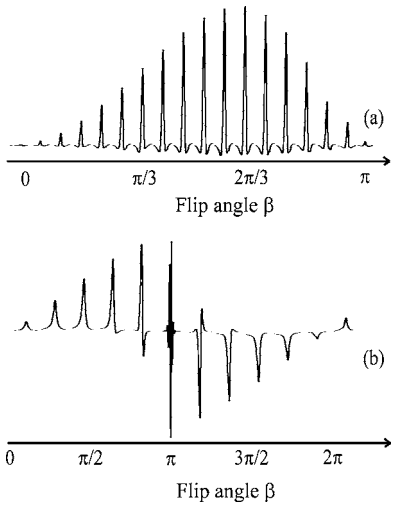

FIG. 4. Spectra vs the flip angle β for a sample with 50% H_2O and 50% D_2O from (a) iDQC CRAZED signals and (b) radiation-damped signals. In iDQC spectra the peak height, but not the linewidth and phase, varies with β, while in radiation-damped spectra they all vary with β.

C. Peak height

Since the approximation of weak dipolar field effects $\xi = \gamma\mu_0 M_0 t e^{-\pi/T_2} e^{-(k^2D+1/T_1)t}\sin\beta \ll 1$ is satisfied in most real systems, one may only retain the $j=0$ terms in the Bessel Taylor expansions of Eqs. (3) and (4).[9,31] Therefore, under the approximation of weak dipolar field effects, the peak height of an absorption mode spectrum related to n-quantum coherence can be further expressed as[32]

$$S(\omega_0)|_{n>0}^{\text{absorb}} = \frac{(-1)^n(\gamma\mu_0 e^{-\pi/T_2}\sin\beta)^{n-1}(1-\cos\beta)}{2^n\left\{\frac{1}{T_2} + (n-1)[k^2D + 1/T_1]\right\}^n} M_0^n, \tag{7}$$

$$S(\omega_0)|_{n=0}^{\text{absorb}} = \frac{\gamma\mu_0 e^{-\pi/T_2}\sin\beta\cos\beta}{2\left\{\frac{1}{T_2} + [k^2D + 1/T_1]\right\}^2} M_0^2. \tag{8}$$

For an absorption mode spectrum related to n-quantum coherence, the peak height is dependent on the flip angle β and nth power of the magnetization M_0. We have

$$S(\omega_0)|_{n>0}^{\text{absorb}} \propto M_0^n \sin\beta^{n-1}(1-\cos\beta), \tag{9}$$

TABLE I. Theoretical linewidths for different coherence orders. Note: Ph. and Av. stand for phase sensitive and absolute value, respectively.

n	0	1	2	3	4	5
Ph. mode	$0.49/(\pi\lambda)$	$1.00/(\pi\lambda)$	$0.49/(\pi\lambda)$	$0.33/(\pi\lambda)$	$0.25/(\pi\lambda)$	$0.19/(\pi\lambda)$
Av. mode	$1.00/(\pi\lambda)$	$1.73/(\pi\lambda)$	$1.00/(\pi\lambda)$	$0.77/(\pi\lambda)$	$0.64/(\pi\lambda)$	$0.56/(\pi\lambda)$

$$S(\omega_0)|_{n=0}^{\text{absorb}} \propto M_0^2 \sin\beta\cos\beta. \tag{10}$$

Equations (9) and (10) with functional dependence on the flip angle β provide a guide for optimizing iMQC signals, which have been previously confirmed with experiments and calculations based on product operator treatment.[10] The profile of the peak height versus the flip angle is remarkably different from conventional sinusoidal form. The experimental results in Fig. 4(a) show that the optimal flip angle for intermolecular double-quantum coherences (iDQCs) is $2\pi/3$, which has been widely applied in many relevant NMR and MRI experiments.[15,33] Considering a special case of $n=0$ and 2 with the corresponding optimal angles ($\beta=2\pi/3$ for $n=2$, and $\beta=\pi/4$ for $n=0$) in Eqs. (9) and (10), peak heights are proportional to $3\sqrt{3}M_0^2/16$ and $M_0^2/4$, respectively. Peak intensities of iDQCs are about 1.3 times than that of intermolecular zero-quantum coherences (iZQCs), which agree well with our previous conclusions using the product operator derivation.[10,15] For experiments performed with a single-pulse sequence and a well-tuned probe, a saw-toothed profile for the line shape as a function of the flip angle is observed [Fig. 4(b)]. This is the typical feature of radiation-damped signals in the frequency domain, as has been reported by Mao and Ye.[27]

D. Linewidth

With the help of the symbolic programming language MATHEMATICA 4.2,[34] theoretical linewidths (Table I) were obtained by calculating the frequency shift at half-peak height under the first-order approximation of the Bessel Taylor expansion. The results suggest that the linewidth of iDQC signals is about 50% narrower than that of conventional single-quantum coherence (SQC) signals. The coefficients of the expressions in Table I are approximately inversely proportional to the coherence orders. For an absorption mode spectrum related to n-quantum coherence, the linewidth can be expressed under the approximation of weak dipolar field effects as follows:

$$\Delta\nu_{1/2}|_{\text{Ph}} = 1/(n\pi\lambda) = \{1/T_2 + (n-1)[k^2D + 1/T_1]\}/(n\pi) \quad \text{(phase-sensitive mode)}, \tag{11}$$

$$\Delta\nu_{1/2}|_{\text{Av}} = (4^{1/n}-1)^{1/2}/(\pi\lambda) \quad \text{(absolute value mode)}, \tag{12}$$

where $\lambda=\{1/T_2+(n-1)[k^2D+1/T_1]\}^{-1}$. Equations (11) and (12) show that the linewidth is independent of the flip angle β, which is confirmed by the results in Fig. 4(a) as well. The linewidth of iMQC spectra becomes narrower with the increase of coherence orders. All these characteristics can be utilized to determine whether the detected signals are entirely originated from pure iMQCs. The linewidths obtained from the CRAZED experiments with several different gradient strengths are listed in Table II, in which the linewidth ratios between any coherence orders are shown to be in well accord with Eqs. (11) and (12). On the other hand, the linewidth of strongly radiation-damped signals depends on the flip angle [Fig. 4(b)].[27,28] Only when the flip angle is infinitely small, the line shape of strongly radiation-damped signal is Lorentzian with a linewidth described by $(\pi T_r)^{-1}$, where T_r is the radiation-damping time.[24,27] Otherwise the lines are narrower than $(\pi T_r)^{-1}$. The bigger the flip angle, the smaller the linewidth [Fig. 4(b)].[27] When the flip angle approaches to π, the line shape turns to infinitely oscillating [Fig. 5(b)].

E. Phase

The phases of iMQC spectra are distorted due to the cosine terms [see Eqs. (a11) and (a12) in the supplementary material for details[32]]. The cosine function is constantly oscillating with a varied frequency. With the increase of coherence order, phase distortion by the cosine factor becomes more serious. The phase distortion of strong radiation-damped signal is also due to the cosine function existing in

TABLE II. Linewidths for different coherence orders obtained from the CRAZED experiments.

	$G=0.94\times10^{-2}$ T m^{-1}		$G=1.41\times10^{-2}$ T m^{-1}		$G=1.88\times10^{-2}$ T m^{-1}	
n	Ph. mode (Hz)	Av. mode (Hz)	Ph. mode (Hz)	Av. mode (Hz)	Ph. mode (Hz)	Av. mode (Hz)
0	1.01	2.18	0.98	2.04	0.94	1.84
1	1.85	3.36	1.89	3.43	1.92	3.49
2	0.96	2.00	0.94	1.94	0.92	1.90
3	0.66	1.59	0.65	1.56	0.63	1.55
4	0.53	1.46	0.52	1.40	0.55	1.38
5	0.46	1.41	0.47	1.30	0.48	1.28

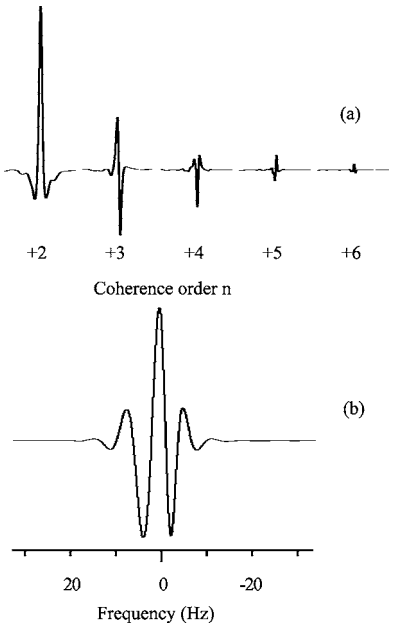

FIG. 5. Phase variations from measurements for (a) n-quantum ($n=2$, 3, 4, 5, and 6) iMQC signals and (b) radiation-damped signals for a sample with 50% H_2O and 50% D_2O. Note the $\pi/2$-phase difference for the adjacent quantum [for instance, $(n+1)$- and n-quantum coherences] iMQC signals. For radiation-damped spectra, when the flip angle is near π, the phase becomes significantly distorted and with great oscillations.

its line-shape expression.[27] However, it is a function oscillating at a fixed frequency. The phase distortion arises from the rising part of the FID envelope. If the FID simply decays, the phase distortion would never be observed.[28] In a single-pulse experiment with strong radiation damping, phase is distorted only when the flip angle is greater than $\pi/2$. When the flip angle is close to π, the phase distortion becomes significant, consistent with the experimental observation [Fig. 5(b)].[27] Note that the phase distortion does not always appear if radiation-damping is not strong enough to become the dominant mechanism for the magnetization to recover to the equilibrium state (for example, when the radiation-damping time is greater than or equal to the longitudinal relaxation time, the phase distortion becomes obscure). This is quite different from iMQCs where the phase distortion always exists. The term i^{-n-1} in Eqs. (5) and (6) indicates that there is a $\pi/2$ phase difference [Fig. 5(a)] for the adjacent coherence order [i.e., $(n+1)$- and n-quantum coherences]. This feature may help for designing phase cycling scheme to select iMQC signals of the desired coherence order. Moreover, for a given order n, there is a π-phase difference between signals purely arising from the adjacent multispin terms in the equilibrium density matrix and properly designed experiments can detect these multispin signals.[9,35]

III. NUMERICAL SIMULATIONS AND EXPERIMENTAL CONSIDERATIONS

In order to further verify the validity of our line-shape theory, the characteristics of the resonance line shape predicted by the analytical calculations were compared with numerical simulations and experimental observations, respectively. For comparison, the amplitudes of all spectra were

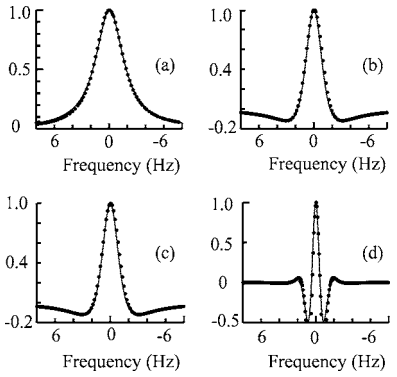

FIG. 6. Comparisons of the spectra from theoretical prediction (solid lines) and numerical simulation (dot lines). The selected coherence orders are (a) $n=1$, (b) $n=2$, (c) $n=0$, and (d) $n=5$, respectively.

normalized. Here the modified Bloch equation with a nonlinear dipolar field term was used in numerical simulations. The transversal and longitudinal relaxations were taken into account, but the diffusion and radiation damping were omitted to make the calculations more tractable. The simulation codes were developed in C++ language.[36] The parameters used in the simulation were as follows: evolution time τ of 3.3 ms to minimize the longitudinal relaxation effects during the evolution period; the transverse relaxation of 0.1 s; τ_d was assumed to be 77 ms; and the amplitude and duration of the iMQC-selection gradient were 0.05 T/m and 3 ms, respectively. The near perfect agreements between the spectra from the numerical calculation and analytical solution, as shown in Fig. 6, demonstrate that the line-shape expressions presented herein are applicable. In addition, the simulated linewidths accord with Eqs. (11) and (12).

Experiments were implemented on a Varian Unity$^+$ 500 spectrometer equipped with self-shielded z-gradient coils and 5-mm HCN triple-resonance rf coil. The probe provides a linear gradient field up to 0.3 T/m in the z direction and all ^{1}H NMR spectra were recorded at 298 K. A typical set of experimental parameters were as follows: a relaxation delay (RD) of 30 s to allow the spin system to completely return to the equilibrium state and prevent any possible stimulated echoes; an evolution time τ of 3 ms to minimize signal at-

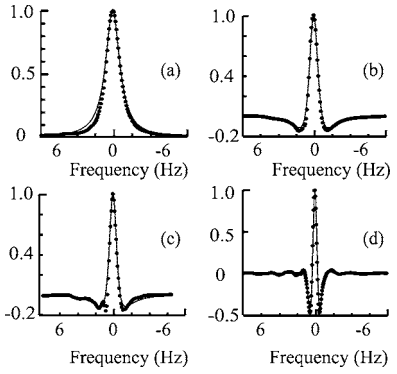

FIG. 7. Comparisons of the spectra from theoretical prediction (solid lines) and experiments (dot lines). The sample is the same as that in Fig. 2. The selected coherence orders are (a) $n=1$, (b) $n=2$, (c) $n=0$, and (d) $n=5$, respectively. The linewidth values which were used for the numerical calculation are listed in Table II.

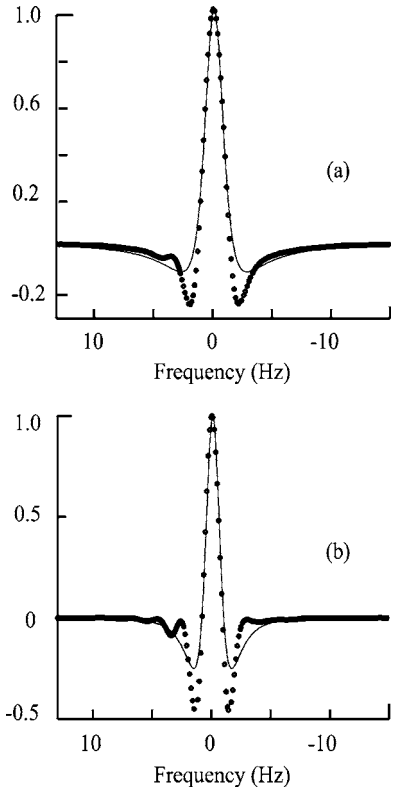

FIG. 8. Comparisons of the theoretical spectra of (a) second-order and (b) third-order iMQCs and experimental data acquired with the probe best tuned (i.e., under the strong radiation-damping condition). The disagreements between theoretical and experimental line shapes at the negative-amplitude regions mostly result from the radiation-damping effects.

tenuation due to diffusion, transverse relaxation, and other effects; and a gradient with a duration $\delta=3$ ms. Radiation-damping effects were effectively suppressed during the evolution period when the transverse magnetization M_{xy} was rapidly dephased by the field gradient immediately following the first rf pulse, and minimized during the detection period by detuning the rf coil, with the duration of the $\pi/2$ rf pulse extended to 140 μs. A sample with 50% D_2O/50% and H_2O was used. The SQC longitudinal relaxation time is about 4.50 s and transverse relaxation time is 1.46 s. The molecular diffusion rate of SQC is 1.59×10^{-9} m^2 s^{-1}. A good shimming environment was necessary in order to get a good line shape. Due to the influence of the magnetic inhomogeneities and other uncertain factors, we used the experimental linewidths (Table II) instead of the parameter λ to fit the line-shape curves. As shown in Fig. 7, the measured spectra and the spectra calculated numerically with experimental input agree reasonably with each other.

IV. ADDITIONAL CONSIDERATION OF LINE SHAPE INFLUENCED BY RADIATION DAMPING

Figures 8(a) and 8(b) present some typical theoretical and experimental spectra when the probe is best tuned and matched. In such case, the radiation-damping effect is very strong. The experimental resonance line shape at the negative-amplitude regions seems to be inconsistent with our theoretical predictions. However, by systematically tuning the probe to different degrees, we found that the better the tuning, the stronger the radiation damping, and the heavier the drop of iMQC spectra at the negative-amplitude regions. Therefore, the disagreements in Figs. 8(a) and 8(b) are mainly due to the radiation-damping effects. In practical experiments related to iMQCs, radiation damping may not be completely suppressed by the field gradient or probe detuning. Hence how the radiation damping influences the iMQC spectra is worth further thorough investigation. Moreover, one can judge whether the detected signals are influenced by radiation damping by comparing the negative-amplitude regions between the theoretical and experimental resonance lines.

V. SUMMARY

In this contribution, explicit analytical expressions for iMQC line shapes of different coherence orders were derived. With the approximation of weak dipolar field effects, the corresponding features of line shape, such as peak height, linewidth, and phase, were investigated in detail. All these features were confirmed by numerical simulations and experimental measurements. The excellent agreements between theoretical predictions, numerical calculations, and experimental observations indicate that the line-shape expressions may be employed to quantitatively interpret the iMQC spectra and to better understand the iMQC effects. In addition, the line-shape features can be utilized as a criterion to judge whether the detected signals are solely originated from iMQCs and not influenced by other uncertain factors.

Due to the similarity of the line shapes and signal features between iMQC and radiation-damped signals in highly polarized liquid-state NMR experiments, detailed comparisons were carried out on peak heights, linewidths, and phases between these two effects. All the results demonstrate that iMQCs and radiation damping result from two different physical mechanisms.

ACKNOWLEDGMENTS

This work was supported by the NNSF of China under Grant Nos. 10234070 and 10375049, NCET and EYTP of Ministry of Education of China, and NIH under Grant No. NS41048.

[1] W. S. Warren, W. Richter, A. H. Andreotti, and B. T. Farmer II, Science **262**, 2005 (1993).
[2] S. Vathyam, S. Lee, and W. S. Warren, Science **272**, 92 (1996).
[3] W. S. Warren, S. Ahn, M. Mescher *et al.*, Science **281**, 247 (1998).
[4] R. T. Branca, S. Capuani, and B. Maraviglia, Concepts Magn. Reson. **21A**, 22 (2004).
[5] G. Deville, M. Bernier, and J. M. Delrieux, Phys. Rev. B **19**, 5666 (1979).
[6] D. Einzel, G. Eska, Y. Hirayoshi, T. Kopp, and P. Wolfle, Phys. Rev. Lett. **53**, 2312 (1984).
[7] R. Bowtell, R. M. Bowley, and P. Glover, J. Magn. Reson. (1969-1992) **88**, 643 (1990).
[8] Q. H. He, W. Richter, S. Vathyam, and W. S. Warren, J. Chem. Phys. **98**, 6779 (1993).
[9] S. Lee, W. Richter, S. Vathyam, and W. S. Warren, J. Chem. Phys. **105**, 874 (1996).
[10] Z. Chen, Z. W. Chen, and J. Zhong, J. Chem. Phys. **115**, 10769 (2001).
[11] S. Ahn, S. Lee, and W. S. Warren, Mol. Phys. **95**, 769 (1998).
[12] J. Jeener, A. Vassenbroek, and P. Broekaert, J. Chem. Phys. **103**, 1309 (1995).

[13] J. Jeener, in *Encyclopedia of Nuclear Magnetic Resonance*, edited by D. M. Grant and R. K. Harris (Wiley, New York, 2002), Vol. 9, p. 642.
[14] J. Jeener, J. Chem. Phys. **112**, 5091 (2000).
[15] J. Zhong, Z. Chen, and E. Kwok, Magn. Reson. Med. **43**, 335 (2000).
[16] S. Capuani, M. Alesiani, R. T. Branca, and B. Maraviglia, Solid State Nucl. Magn. Reson. **25**, 153 (2004).
[17] R. R. Rizi, S. Ahn, D. C. Alsop *et al.*, Magn. Reson. Med. **43**, 627 (2000).
[18] C. Ramanathan and R. W. Bowtell, Phys. Rev. E **66**, 041201 (2002).
[19] R. Bowtell, S. Gutteridge, and C. Ramanathan, J. Magn. Reson. **150**, 147 (2001).
[20] Z. Chen, Z. W. Chen, and J. Zhong, J. Am. Chem. Soc. **126**, 446 (2004).
[21] J. Jeener, Phys. Rev. Lett. **82**, 1772 (1999).
[22] Y. Y. Lin, S. Ahn, N. Murali, W. Brey, C. R. Bowers, and W. S. Warren, Phys. Rev. Lett. **85**, 3732 (2000).
[23] N. Bloembergen and R. V. Pound, Phys. Rev. **95**, 8 (1954).
[24] X. A. Mao and C. H. Ye, Concepts Magn. Reson. **9**, 173 (1997).
[25] Y. Y. Lin, N. Lisitza, S. D. Ahn, and W. S. Warren, Science **290**, 118 (2000).
[26] S. Y. Huang, C. Anklin, J. D. Walls, and Y. Y. Lin, J. Am. Chem. Soc. **126**, 15936 (2004).
[27] X. A. Mao and C. H. Ye, J. Chem. Phys. **99**, 7455 (1993).
[28] X. A. Mao and J. X. Guo, Phys. Rev. B **49**, 15702 (1994).
[29] C. Ramanathan and R. Bowtell, J. Chem. Phys. **114**, 10854 (2001).
[30] J. D. Walls, F. K. H. Phoa, and Y. Y. Lin, Phys. Rev. B **70**, 174410 (2004).
[31] P. M. Morse and H. Feshbach, *Methods of Theoretical Physics* (McGraw-Hill, New York, 1953).
[32] See EPAPS Document No. E-JCPSA6-123-022529 for the complex FT on iMQC time-domain expressions and the check on the correctness of Fourier transform. This document can be reached via a direct link in the online article's HTML reference section or via the EPAPS homepage (http://www.aip.org/pubservs/epaps.html).
[33] J. Zhong, Z. Chen, and E. Kwok, J. Magn. Reson Imaging **12**, 311 (2000).
[34] MATHEMATICA, Version 4.2, Wolfram Research, Inc., Champaign, IL, 2002.
[35] Z. Chen, Z. W. Chen, and J. Zhong, J. Chem. Phys. **117**, 8426 (2002).
[36] C. B. Cai, Z. Chen, S. H. Cai, and J. Zhong, J. Magn. Reson. **172**, 242 (2005).